Discrete Dynamic Equilibrium Model for a Complex Problem of Flutter Interactions

Ichiro Ario[a,*]

[a]*Department of Civil and Environmental Engineering, Hiroshima University, Higashi-Hiroshima, 739-8527, Japan*

Abstract

The dynamic bifurcation analysis of the nonlinear oscillation of a simple fluidelastic structure is presented. This structure is a cantilever beam in a flow, and it behaves as a nonlinear system without potential energy. The structure demonstrates complex flutter behaviour that varies with the controlled flow velocity. We observe the flutter behaviour in a flow experiment, and the motion is characterised with this present model based on chaos theory of discrete dynamics. We can readily find the solution of the simple system, with which it is possible to create a map of the complex flutter behaviour.

Keywords: Dynamic systems, Dynamic instability, Nonlinear mechanic model, Bifurcation theory, Discrete equilibrium model

1. Introduction

In flexible structures such as suspension bridges and/or membrane domes, there is a dangerous possibility that the structure develop a dynamically unstable vibrational response at a critical wind velocity [1, 2]. The structural instability in this fluid-structure interaction involves a complex behaviour as a result of various factors, and there have been theoretical approaches developed for understanding the mechanism of its occurrence. However, a stability criterion based only on static energy is thought to be of no value because the fluid dynamic load is a non-conservative field with no associated potential function[3]~[10].

General non-conservative systems have been investigated by Plaut[11, 12], and Huseyin[13] has made progress in the nonlinear analysis of non-conservative systems using a perturbation method. Huseyin investigated spontaneous divergence and bifurcation into flutter and the stability of the equilibrium path in generalised structures by means of successive diagonalisations[14] and similar successive transformations into a standard Jacobian form. Novak[15] showed that the typical dynamic instability resulting from the effect of the fluid

*Corresponding author.
Email address: mario@hiroshima-u.ac.jp (Ichiro Ario)

dynamic coefficient $C(\alpha)$ and a dynamic bifurcation phenomenon involving an amplitude jump (i.e., a singularity). Additionally, Parkinson and Smith[17] compared the nonlinear behaviour in experimental and analytical results by analysing the polynomially approximated coefficient $C(\alpha)$ obtained from its experimental value. Thus, it can be seen that geometrical and static stability criteria for divergent vibrations such as flutter cannot be treated under a non-conservative load; for this reason, a powerful analytical method to replace this approach has been sought[18, 19].

There are two primary numerical approaches for the analysis of flutter in solid frames: the modal analysis method, which combines the characteristic vibrational modes, and the direct flutter analysis method, which directly solves the equations of motion involving continuous fluid forces. Modal analysis is based on the assumption that the characteristic vibrational mode during flutter can be expressed with sufficient accuracy as a linear summation of several characteristic vibrational modes for the structure under consideration. However, it has the weakness that it cannot be applied to phenomena with strong nonlinear effects. Additionally, because the accuracy of direct flutter analysis depends on the specific flutter mode and on the transient fluid characteristics, a large-scale computation is necessary. The accuracy of the computation depends on the available computational power[20]~[23], making it difficult to pinpoint the essential cause of the unstable behaviour. Recently, computational fluid analyses (CFD) based on the Navier-Stokes equations have been performed. There are numerous research activities analysing the flow around objects, and progress is also being made on three-dimensional transient systems with fluid-structure interaction[24]. Problems as complex as Kármán vortex excitation can be accurately reproduced [25, 26]. However, there are numerous challenges to their solution, such as the use of the analytical mesh, the modelling and unified expression from laminar flow to turbulent flow, and the incorporation of moving boundary conditions. In order to forecast this problem using computing methods, we need detailed large-scale calculations, since the solutions of various behaviours appear chaotic such as strange attactor, limit cycle and so on [27]~[31].

In this research, we do not regard the problem of fluid-structure interaction from the viewpoint of computational fluid dynamics. Instead, focusing on the structural instability occurring in the non-potential system from the viewpoint of elastohydrodynamics, we devise a nonlinear equation that is universally applicable to problems such as our primary challenge, which is understanding the behaviour near the (double-period) critical flow velocity. The advantage of this approach is its ability to predict stability when the repeated equilibrium condition is satisfied under a certain fluid dynamic force or to predict the occurrence of instability involving flutter when the condition is not satisfied. To develop a computational method based on discrete dynamics to understand flutter in a model with fluid-structure interactions under a non-conservative field, we considered the system of a rigid body and a rotary spring under a uniform flow field. We verified the occurrence of flutter by varying the flow velocity in an open-channel experiment in which we observed and measured the self-oscillatory response. The main achievement of this work is that we not only recognise the essential behaviour of this problem (i.e., the instability under a non-conservative field that has been said to be of no useful in the static situation), but we

also develop an approximate nonlinear analysis method and verify its ability to produce results similar to the observed results. It is important from the engineering point of view to investigate the qualitative changes in the behaviour of a basic system with the goal of understanding dynamic instabilities.

2. Self-oscillation under a non-conservative fluid dynamic load

In this paper, we discuss purely elastohydrodynamic instability under an fluid dynamic load by considering the stall galloping flutter phenomenon arising from self-oscillation in a system with one degree of freedom. Flutter phenomena are often found in the field of aerodynamic or hydrodynamic engineerings; for example, the flutter of a main wing is a typical, non-steady-state problem concerning elastic stability. Recent work has shown that the panel flutter and the chaos found in flat panels and shell structures placed in a supersonic flow field are the same type of problem[32].

2.1. Elastohydrodynamic instability

The object is constrained to move only in the direction normal to the force of the flow as following in [16]. The displacement from the equilibrium position is expressed by the generalised coordinate y. The object is supported by a spring with an elastic stiffness k and a damping force, $c\dot{y}$, proportional to the velocity, $\dot{y}$. The velocity of the fluid relative to the object, v_R, is given by the vector sum of the constant horizontal velocity, v, and the response velocity, $\dot{y}$, and the relative velocity v_R for the angle gives rise to the vertical force component F_v :

$$F_v = \frac{1}{2}\rho v^2 a C(\alpha) \tag{1}$$

where ρ is the fluid density and a is the projected area of the front face of the object. Under the quasi-steady-state assumption, the coefficient C depends only on the angle, given by $\alpha = \tan^{-1}(\dot{y}/v)$. For large values of α, C is expected to be negative. When C and $\dot{y}$ have the same sign, the fluid dynamical force has the effect of amplifying the initial movement; thus, wind, for example, can be regarded as producing negative damping. Expanding C, we obtain

$$C(\alpha) = A_1\left(\frac{\dot{y}}{v}\right) - A_3\left(\frac{\dot{y}}{v}\right)^3 + A_5\left(\frac{\dot{y}}{v}\right)^5 - A_7\left(\frac{\dot{y}}{v}\right)^7 \tag{2}$$

and the elastohydrodynamic equation of motion is expressed as

$$m\ddot{y} + c\dot{y} + ky = \frac{1}{2}\rho v^2 a C(\alpha) \tag{3}$$

If we regard $\dot{y}/v$ as sufficiently small relative to small vibrations, only the first term of the expansion of C will remain, and the effective damping coefficient multiplying $\dot{y}$ becomes

$$c - \frac{1}{2}\rho v^2 a \frac{A_1}{v} \tag{4}$$

Because A_1 for the object is known from experiments to be positive, the critical flow velocity for the actual damping force for which (4) becomes zero is given by

$$v_{\mathrm{cr}} = \frac{2c}{\rho a A_1} \tag{5}$$

Below v_{cr}, the initial external disturbance decays over time. Above v_{cr}, however, even a small external disturbance becomes amplified by the negative resistance and, thus, the vibration diverges. Therefore, the trivial equilibrium solution $y = 0$, which is true for all v, becomes unstable at this critical flow velocity. When the load exceeds this critical flow velocity, the vibration should grow indefinitely according to the linear theory; in reality, however, a finite limit cycle arises due to the higher-order terms in the expansion of C. According to the quasi-steady-state theory, the occurrence of galloping depends on the fluidelastic force $C_{Fy}(\alpha)$; however, the characteristics of the static fluid dynamic force are determined by the interference between the separating shear layer and the wake field.

2.2. Structural vibration due to fluid dynamic forces

Kármán vortices form downstream of a non-streamlined object in a fluid. Because of the periodic shedding of vortices into the wake region, various periodic fluid-dynamic-forces are exerted on the structure. The observation of the vortex-induced vibration of a two-dimensional cylinder reveals that the vortices released above a certain vibrational amplitude are induced by the vibration of the cylinder itself. When the amplitude suddenly increases beyond the resonant flow velocity, the frequency component corresponding to the vortex shedding vanishes, and the structure starts a steady-state vibration at a single frequency. Known as "frequency locking", this phenomenon is characteristic of the nonlinearity of the vortex-induced vibration. According to the traditional explanation, the vortex-induced vibration is a forced vibration caused by Kàrmàn vortices and is a resonant phenomenon. As seen from the frequency-locking phenomenon, however, it is inaccurate to regard the vortex-induced vibration as a forced vibration caused by the vortices, because the vortices initiating the vibration are attenuated by the vibration of the object itself. For this reason, there is an increasing tendency to regard the phenomenon as a type of self-induced oscillation in the system of the interacting object and fluid. However, formalising this vibration phenomenon is generally difficult.

3. Observation of flutter in an open channel experiment

In this section, we describe the configuration of the model for the structure-fluid interaction in an open water channel experiment to reproduce flutter. We examine the flutter phenomenon by varying the flow velocity and visualising the response by video recording.

3.1. Outline of the experiment

The experiment was conducted in a rectangular open channel made of acrylic, which was 10 m long, 60 cm wide, and 15 cm deep with an incline of 1/1000. The test object was placed slightly above the bottom so that friction with the surface would not influence

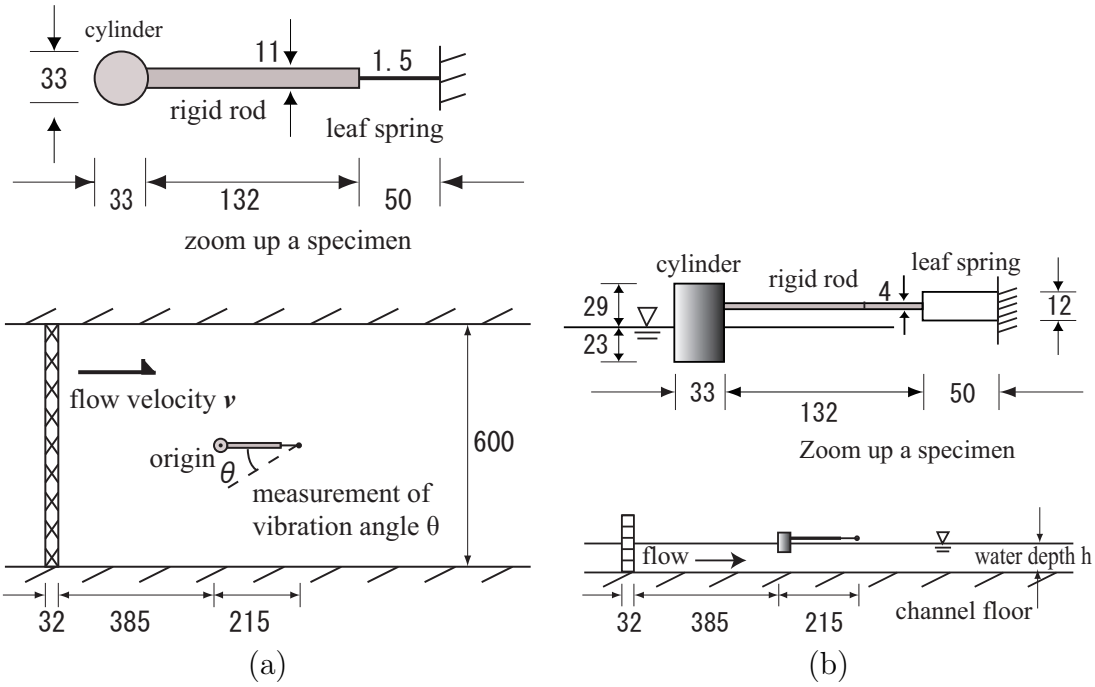

Figure 1: Schematic diagram of the experiment; (a) plane view, (b) side view

the experiment when the object vibrated. A full-width(b), variable-height(h) dam was placed at the bottom of the channel to control the water level. In the channel experiment facility, the average flow velocity $\bar{v}$ of $\bar{v} = Q/(hb)$ was obtained by controlling the height h, rather than by varying the flow rate Q of the supplied water. We varied the flow velocity by controlling the water level and measured the angle and period of vibration of the test object. To make the flow around the test object as uniform as possible, we placed a honeycomb that was 3.2 cm thick, 60 cm wide, 15 cm high, and 4 mm in diameter as a flow regulator on the upstream side of the test object. The test object consisted of a plastic cylinder (5.2 cm high and 3.3 cm diameter), a thin acrylic leaf spring (5 cm long), and a rigid wooden rod (1.1 cm wide, 0.4 cm high, and 13.2 cm long). Adjusting the height of the cylindrical test object while maintaining a constant projected area of the object within the fluid, we immersed only the plastic cylinder at the end of the structure into the water. All motion of the test object was fixed except for the rotation in the horizontal plane. The experimental channel, the test object, and the placement of the object are shown in **Fig.** 1.

3.2. Material properties and flow parameters

A lightweight material was chosen for the test object to produce a large vibrational response. The test object was constructed by combining acrylic sheet stock for the rotary spring, wood for the rigid rod, and plastic for the cylinder. The rotary spring was a thin vertical acrylic sheet whose flexion constrained the motion of the test object to rotation in the horizontal plane. The spring constant of the rotary spring was determined by

Table 1: Material property of a specimen

Mass (g)	26.89
Length between the center of a cylinder and the support(cm)	19.85
The projected area of a cylinder (cm^2)	7.59
Inertia moment (kgm^2)	0.00157
Stiffness for a rotary spring (Nm)	0.00276
Damping parameter (Nm.sec)	0.00033

Table 2: Flow velocity data for the open channel experiment

Case	water depth (cm)	flow velocity (cm/sec)	Re number	Case	water depth (cm)	flow velocity (cm/sec)	Re number
1	9.7	0.47	130	11	8.0	6.8	2338
2	10.1	1.65	458	12	7.7	7.1	2441
3	10.7	3.94	1108	13	7.1	7.7	2647
4	6.1	6.91	1944	14	5.9	9.3	3186
5	4.3	9.80	2758	15	5.1	10.7	3686
6	11.2	4.9	1684	16	4.8	11.4	3919
7	10.2	5.4	1856	17	4.3	13.3	4572
8	9.6	5.7	1959	18	3.9	14.0	4813
9	9.2	5.9	2028	19	3.4	16.1	5534
10	8.5	6.4	2200	20	2.9	18.9	6497
				21	2.5	21.9	7528

measuring the static load versus bending, and the object's inertial moment was calculated from $I = m\ell^2$. The damping coefficient of the model was obtained from the free damped oscillation, $(2\sqrt{kmh})$. These parameters are shown in **Table** 1. To capture the flutter behaviour, the experiment was conducted at 21 flow velocities as shown in **Table** 2. The flow velocities in **Table** 2 are the average cross-sectional flow velocity made uniform by the honeycomb.

3.3. Experimental results and discussion

The vibration of the circular cylinder was visualised as shown in **Fig.** 2. Using still images taken at 30 frames per second, we measured the angle of the vibration at each instant. Interpolating the angular response data and taking derivatives, we obtained angular velocity and angular acceleration. The left side of the channel was defined to be the positive direction. Because the fluid dynamic force was acting continuously and stopping the flow was not possible, we commenced the measurement once the flow became steady at a certain level.

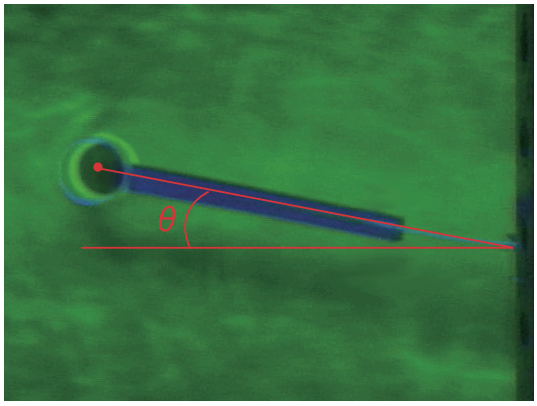

Figure 2: Experimental state related between a specimen and water flow

3.3.1. Vibrational response results

In **Fig.** 3, we show the time series of the angular amplitude for typical flow velocities. The critical velocity in this open channel experiment has the same physical meaning as in equation (5). Because it was difficult to measure exactly, the critical velocity was taken to be the flow velocity immediately before the test object started to vibrate; this flow velocity was 6.4 cm/sec (Re=2200) in case 10. Below the critical velocity, the test object remains still and barely vibrates. Slightly above the critical velocity (6.8 cm/sec) in case 11, the test object exhibits a steady vibration, and as the flow velocity increases, both the angular amplitude and frequency increase as in an ordinary vibrational phenomenon. As the flow velocity is increased still further, however, the angular amplitude generally decreases; additionally, the regularity is lost and the angular amplitude and the period change over time.

In case 21, wherein the flow velocity (21.9 cm/sec) and thus, the hydrodynamic force were the greatest, the test object did not return to the original position; it instead vibrated in a tilted position. From this result, it is clear that instability occurs in the vibrational response in the high flow-velocity regime.

3.3.2. Bifurcation due to increasing flow velocity

The test object barely vibrated at velocities below the critical flow velocity; however, in the low flow-velocity regime above the critical velocity, the test object exhibited a steady vibration. In other words, the regular vibrational response emerged from the motionless state at the critical velocity. In **Fig.** 4, we show plots of the experimental values for the angular amplitude (maximum and minimum) over six periods and the theoretical values from an averaging method. The result of the averaging method is similar to the experimental result immediately after the bifurcation, but the results deviate significantly afterwards. In the high flow-velocity regime above the critical velocity, the vibration of the test object became non-periodic and exhibited irregular responses in which the angular amplitude varied between small and large values. We also observed a response with a large vibration following a state with no vibration. When the flow velocity was increased

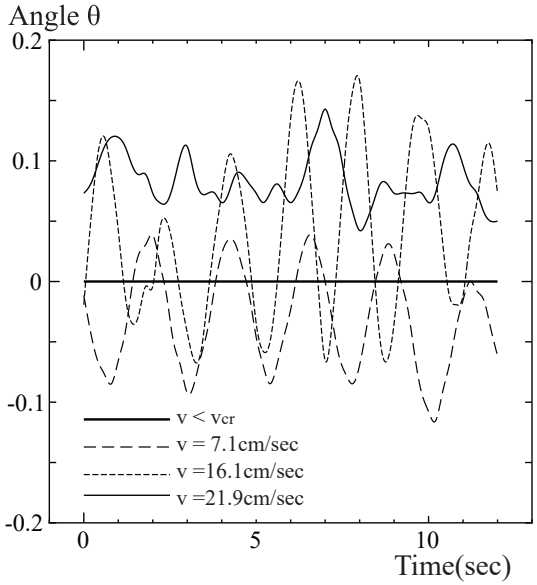

Figure 3: Instability in the angular response due to increasing flow velocity

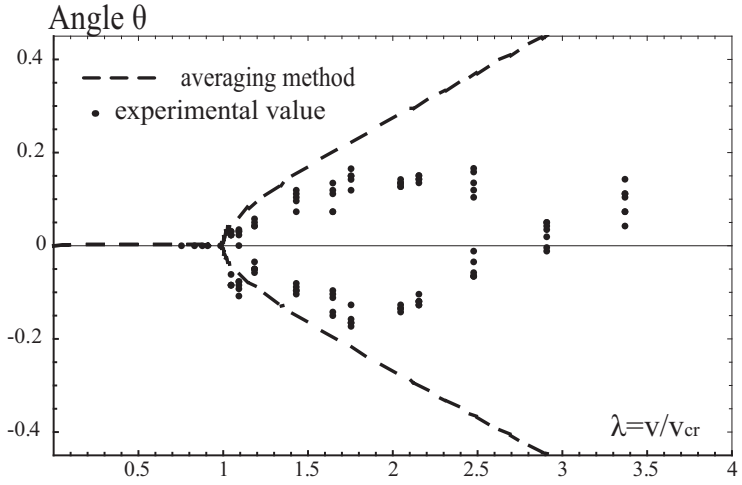

Figure 4: Bifurcation of the angle due to increasing flow velocity

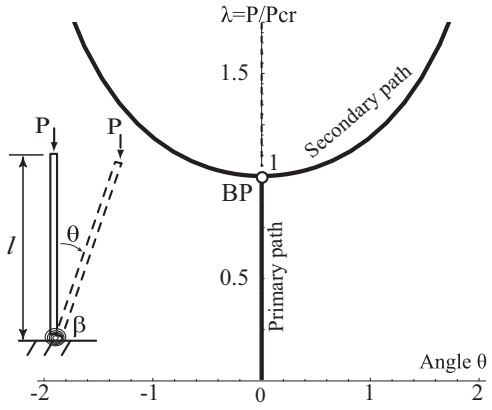

Figure 5: An example of pitchfork bifurcation buckling

further, the test object vibrated while maintaining a tilted position, exhibiting flutter. The averaging method (Refer to Appendix A), the results of which are shown as a broken line in **Fig.** 4, is an analytical method that gives the amplitude of the angular vibration by averaging $\theta(t)$ over one period, assuming that $\theta(t) = A\sin(\omega t + \varphi)$. Here, A, ω, φ, t are the amplitude, the characteristic angular frequency, the phase difference, and time, respectively. In **Fig.** 4, the averaging method results show an increasing deviation from the experimental values with increasing flow velocity. However, the experimental angular amplitude starts to decrease, rather than increase, when the flow velocity exceeds a certain value, departing significantly from the averaging method results. Thus, it is not possible to model these behaviours by this method in the high flow-velocity regime.

4. Static bifurcation and discrete dynamics

In this section, we employ a simple static bifurcation model and outline the concept of discrete mechanics used in chaos theory. We also describe the model's properties and present a method that gives an approximate solution for flutter.

4.1. An example of static bifurcation

Here, we discuss the bifurcation phenomenon in a system with one degree of freedom in which a vertical load P acts on a rigid rod with a spring stiffness β. This one-degree-of-freedom model consisting of a rigid body and a rotary spring is shown in the left portion of **Fig.** 5. The total potential energy for this system, $\mathcal{U}$, is expressed as

$$\mathcal{U} = \frac{1}{2}\beta\theta^2 - P\ell(1 - \cos\theta). \tag{6}$$

In this equation, the first term is the strain energy of the spring, and the second term is the external force potential energy.

By the principle of stationary potential energy, the equilibrium condition is given by

$$\frac{\partial \mathcal{U}}{\partial \theta} = \beta\theta - P\ell \sin\theta = 0 \tag{7}$$

Therefore, the equilibrium condition for the system becomes

$$\theta = 0, \quad \text{or } P = \frac{\beta\theta}{\ell \sin\theta} \tag{8}$$

$\theta = 0$ satisfies equation (7) regardless of the value of P and is a trivial solution indicating the equilibrium of the rigid body in the vertical position.

However, taking θ in equation (8) to the limit,

$$\lim_{\theta \to 0} \frac{\theta}{\sin\theta} = 1$$

we obtain

$$P = P_{\text{cr}} = \frac{\beta}{\ell}. \tag{9}$$

The rod bifurcates and begins to tilt from the vertical position ($\theta = 0$) at P_{cr}; this P_{cr} is called the buckling load.

By defining the nondimensional load parameter

$$\lambda \equiv \frac{P}{P_{\text{cr}}} = \frac{P\ell}{\beta} \tag{10}$$

equation (8) is made dimensionless for $\theta \neq 0$, and for the equilibrium path after bifurcation, we have

$$\lambda = \frac{\theta}{\sin\theta}. \tag{11}$$

Fig. 5 shows the relationship between the load parameter λ and the displacement θ. For $\lambda < 1, \theta = 0$ is the primary equilibrium path, and for $\lambda > 1, \lambda = \theta/\sin\theta$ becomes the secondary bifurcation path. $\lambda = 1$ is the critical point as a stable symmetric Bifurcation Point ('BP' marked in **Fig.** 5) , and this system exhibits typical pitchfork bifurcation buckling[35, 36].

4.2. Discrete mechanical systems

We consider a time series in which the variable x describing the state of the system varies as $x_0, x_1, x_2, \cdots$ over the discrete time $t = 0, 1, 2, \cdots$. The value of x_{n+1} in the series can be determined from $x_0, x_1, x_2, \cdots$. We assume that the individual values in the series are described in terms of a function $f(x)$ as

$$x_1 = f(x_0),\ x_2 = f(x_1), \cdots,\ x_{n+1} = f(x_n)$$

If $f(x)$ and the initial value x_0 are known, the discrete solution $x_0, x_1, x_2, \cdots$ can be uniquely determined by mapping. The changing values $x_0, x_1, x_2, \cdots$ of the discrete solution given by this mapping are called a trajectory.

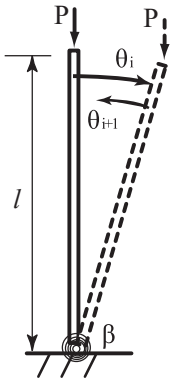

Figure 6: Conceptualisation of equilibrium from a non-equilibrium state

A trajectory is either periodic or non-periodic. A stable periodic point exists in a periodic trajectory. In a non-periodic trajectory, however, the time series starting from the initial value x_0 assumes values within a certain range but never takes the same value twice, and the trajectory becomes unstable.

A point that is not changed by the mapping, namely, a point x^* that satisfies $x^* = f(x^*)$ in the mapping $x_{i+1} = f(x_i)$, is called a stationary point. A stationary point is a solution to the equation $x = f(x)$.

A stationary point is either stable or unstable, and one that attracts nearby trajectories is called a stable stationary point. The stability is unrelated to the global properties of $f(x)$; rather, the stability is determined by the local property of whether the absolute value $|\mathrm{d}f(x^*)/\mathrm{d}x^*|$ of the gradient at the stationary point is greater than 1:

$$\frac{\mathrm{d}f(x^*)}{\mathrm{d}x^*} \begin{cases} < 1: \text{ stable fixed point} \\ > 1: \text{ unstable fixed point} \end{cases} \tag{12}$$

When all of the stationary points are unstable, a periodic point emerges. The points to which the solution returns after being mapped T times, that is, the points $x_0^*, x_1^*, \cdots, x_{T-1}^*$ satisfying

$$x^* = f^T(x^*) = f(f(f(\cdots f(f(x^*))\cdots))) \tag{13}$$

are called $T-$periodic points or $T-$periodic solutions such as recurrence or theorem ergodic theorem, and the corresponding trajectory is called the $T-$periodic trajectory.

The solution to the equation of motion during an actual flutter event is a continuous function in time; however, after discretisation, the solution can be regarded as a vibrational response changing at discrete times $t = 0, 1, 2, \cdots$. Thus, the change in the vibrational response over time can be uniquely determined from the initial state (prior to vibration) and the solution to the equation of motion.

4.3. Equilibrium condition of Time-periodic trajectory approach

The concept of stability is modelled by solving complex nonlinear mechanics such as bifurcations and/or chaos. To do this, our proposed method considers the distance between

two trajectories that start at two adjacent points $x_0,\ y_0 = x_0 + \delta,\ (\delta \ll 1$ is an unknown perturbation in this study) and calculates $\lim i \to +\infty$ for one dimensional discrete dynamical systems $x_{i+1} = f(x_i), i = 0, 1, \cdots$. The two solutions $x_i = f^{(i)}(x_0), y_i = f^{(i)}(y_0)$ after the number i of times are described as

$$\begin{aligned} |y_i - x_i| &= \left|f^{(i)}(y_0) - f^{(i)}(x_0)\right| \\ &= \left|f^{(i+1)}(x_0) - f^{(i)}(x_0)\right| \\ &= |f(x_{i+1}) - f(x_i)| = |\Delta_i|. \end{aligned} \tag{14}$$

If the number i of times is large, the difference of Eq.(14) will be very small. Then, the expression $|y_i - x_i| = 0$ is satisfied, which is defined as the equilibrium state in this paper. Thus, Eq.(14) becomes

$$\lim_{i\to\infty} |f(x_{i+1}) - f(x_i)| = \left|f^{(i+1)}(x^*) - f^{(i)}(x^*)\right| = 0. \tag{15}$$

Then, x^* is the stationary point defined the equilibrium state in this discrete system. If Eq.(15) does not converge, it would indicate a non equilibrium state depending on the T-periodic trajectory x^*. In this discrete method, it is significant to solve this convergent solution x^* from the initial values including the small perturbation, thus obtaining the (in-)stability of the state of the system.

4.4. Flutter analysis using discrete mechanics

In this section, we assume that the steady-state hydrodynamic load depends on the velocity and treat the load as non-conservative and dissipative. We apply this present method in discrete mechanics to the present buckling model under hydrodynamic forces P_i in a similar manner to the system under a static load P modelled with a rotary spring and a rigid rod. We assume that approximate same value for a discrete load as $P = P_i$ but the deformation θ_i depends on time i in this paper. And we assume that the system and the fluid dynamic forces are initially out of equilibrium and that the effect of the dissipating forces, the inertial force, and other forces under such conditions may be understood in terms of Δ_i. In the initial state at time i, θ_i and θ_{i+1} are not equal and there is small difference including a pertubation. Based on Eq.(7) and/or Eq.(14), the present discrete model for the fluid-elastic interaction problem becomes the following non-equilibrium buckling equation :

$$\beta\theta_{i+1} - P\ell \sin\theta_i = |\Delta_i|, \quad i = 0, 1, \cdots \tag{16}$$

In the formula (16), if the counter-clockwise direction is positive, as shown in **Fig.**6, the non-conserved discrete external moment of the ith iteration is negative. In the direction of $-\theta_i$, the internal resistance moment of the $(i+1)$th iteration is the rotational difference $|\Delta_i|$ when its reverse rotation is θ_{i+1}. Here, $|\Delta_i|$ is a measure of the non-equilibrium condition and we assume that $\lim_{(i\to\infty)} |\Delta_i| = 0$; in this paper, the system is defined to be in equilibrium when this condition is met. In other words, if we suppose that i is sufficiently large in equation (16) and the difference Δ_i is negligibly small, we can write a discretised equilibrium equation

$$\beta\theta_{i+1} - P\ell \sin\theta_i = 0 \tag{17}$$

To find a solution that has a mapping form, we solve equation (17) for θ_{i+1} and obtain

$$\begin{aligned} \theta_{i+1} &= \lambda \sin \theta_i \\ &= \lambda(\sin(\lambda \sin(\cdots \theta_0))))) \\ &= f^T(\theta^*) \end{aligned} \tag{18}$$

which is analogous to equation (13). Here, $\lambda = P\ell/\beta$ is an external force parameter. Thus, we have a discrete mechanical system in which θ_{i+1} is uniquely determined as a nonlinear mapping once θ_i is known. In this paper, we apply the concept of this analysis to the flutter observed in this experiment.

5. Analytical results and discussion

5.1. Evaluation of structural instability with period-doubling bifurcation using iterative mapping formula

In this section, we compute the bifurcation diagram based on discrete mechanics and verify the results against the experiment. The existing formalisation based on the analytical theory of elastohydrodynamics, which comprehensively describes the behaviour near the critical flow velocity, can lead to solution curves, as seen in the averaging method. However, understanding or formulating the subsequent higher-order bifurcation and the solution's behaviour is difficult and depends on the stability and complexity of the solution. Instead, we attempt to formulate the problem by considering, as in Section 4.3, the balance that exists in the non-equilibrium state due to the interactions between the hydrodynamic forces and the structural system. Here, we regard the relative flow velocity as a parameter, rather than the relative load as in equation (17), and consider the equilibrium condition from the non-equilibrium state in terms of this relative flow velocity. In a wind tunnel experiment[1, 2] or in a wind-resistant design, the relative flow velocity is a significant physical parameter, whereas evaluating the drag coefficient tends to be difficult when it is expressed in terms of the relative load. Furthermore, assuming that the relative load and the relative fluid velocity can be treated as external force parameters, we can express the regression equation, as in equation (18), as follows:

$$\alpha_{i+1} = \left(\frac{v}{v_{cr}}\right) \sin \alpha_i, \quad i = 0, 1, 2, \cdots \tag{19}$$

For the initial angle α_0, we substitute the value in the vicinity of 0 as in the analytical case. Note that the response α_i will differ from the experimental angle θ_j, and α_i should be regarded as a virtual angular response. **Fig.** 7 compares the experimental results for the angular amplitude in the open channel experiment with the computed bifurcation diagram for increasing flow velocity which has the increment of a parameter $v/v_{\mathrm{cr}} = 0.005$ in the range from 0 to 4.

In the figure, each dot marks an experimental value, and the numerical solutions from the 201st through the 300th iterations of the mapping are matched against the experimental data. Despite the fact that we do not include the physical parameters for the fluid

medium, such as the drag coefficient and the viscosity, and we use only repeated mapping calculations of one dimensional discrete dynamics model, there is similarity between the physical behaviours of the computed results, α_n, and the experimental values, θ_j. Thus, we have a unified approximate equation that exhibits bifurcation and chaotic behaviours in the bifurcation diagram and can also describe the change in the flow state near the critical flow velocity due to the period-doubling bifurcation.

In the experiment, the vibrational response began to be disorderly near $\lambda \geq 2.3$ (corresponding to a flow velocity of 16.1 cm/sec). At first, we observed a convergence into two, rather than one, limit cycles, a phenomenon called secondary bifurcation in discrete mechanics. There was an increase in the angular amplitude following the primary bifurcation, but there was a decreasing trend following the secondary bifurcation (i.e., the branch with the lowest angular amplitude in the bifurcation diagram in **Fig.** 7). Further theoretical investigations will be necessary to explain this observation. Additionally, the vibration angle for flow velocities of 18.9 cm/sec and 21.9 cm/sec ($\lambda \geq 2.8$) was no longer steady and period, and instead it exhibited irregular vibrational responses. These flutter behaviours can be recognised as a higher-order bifurcation phenomenon from discrete mechanics.

Then, the Liapunov exponent[34] means the index of dynamic instability using Liapunov's direct method and the definition of the index shows in the following;

$$\Lambda(x_0, n) \equiv \frac{1}{n} \sum_{t=0}^{n-1} \ln |f'(x_t)|$$

where, it is noted two closed orbits $x_t, x'_t, (t = 0, 1, 2, \cdots)$, a function $f'(x_t)$ depends on x_t, and x_0 is the first given value. If the number n on the above equation increased ∞ as a big number, it would get to a value Λ_∞ in the end, this is the Liapunov exponent value at a parameter. We have computed the Liapunov exponent values corresponding to this bifurcation diagram in **Fig.** 8. The bifurcation point on the bifurcation diagram corresponds to the changing point from a negative value (stable) to a positive value (unstable) in **Fig.** 8 when the incremental parameter v/v_{cr} at the critical value $v/v_{cr} = 1.0$. From this amplitude, the load parameter keeps dynamic instability as the spreading distribution of chaos attarctor.

According to the figure, the exponent vanishes at BP1, BP2, and BP4, which mark the bifurcation points, and near these points a change in the flow state occurs. It is also seen that for $\lambda > 2.6$, the exponent is positive and the system becomes unstable.

The angular results α_i from the bifurcation diagram and the experimental angular values θ_j are, apart from the scale, quite similar in terms of their domains of bifurcation (i.e., the range of the flow velocity over which bifurcation occurs) and their turbulent behaviours. The consistency between the bifurcation diagram and the experimental values shows that, despite the effects of various physical parameters, flutter demonstrates the concept of bifurcation. Bifurcation is a concept common in nonlinear problems, and it is demonstrated in the dotted path in **Fig.** 9. The ability to predict flutter with this method in a top-down and unified manner has a significant merit: it provides important information about the likelihood of the occurrence of these physical phenomena implicit in

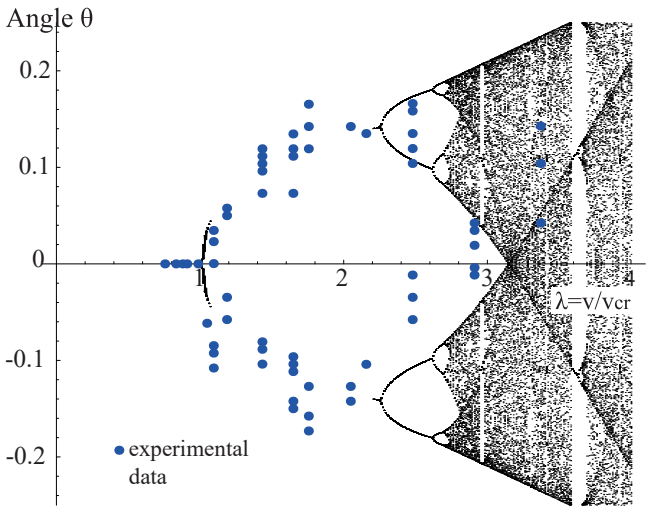

Figure 7: Bifurcation diagram and experimental results for the maximum angular amplitude due to the change in flow velocity.

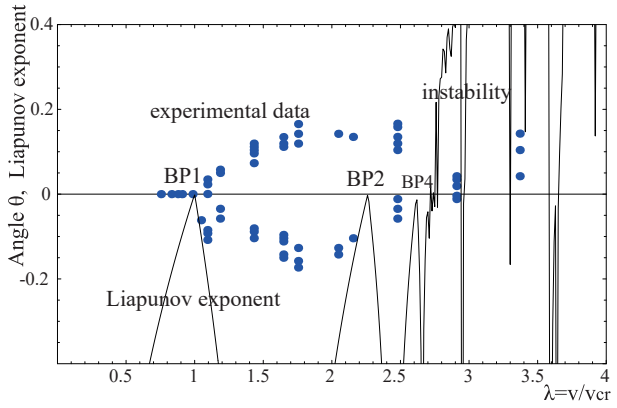

Figure 8: Relationship between the experimental values and the Liapunov exponent.

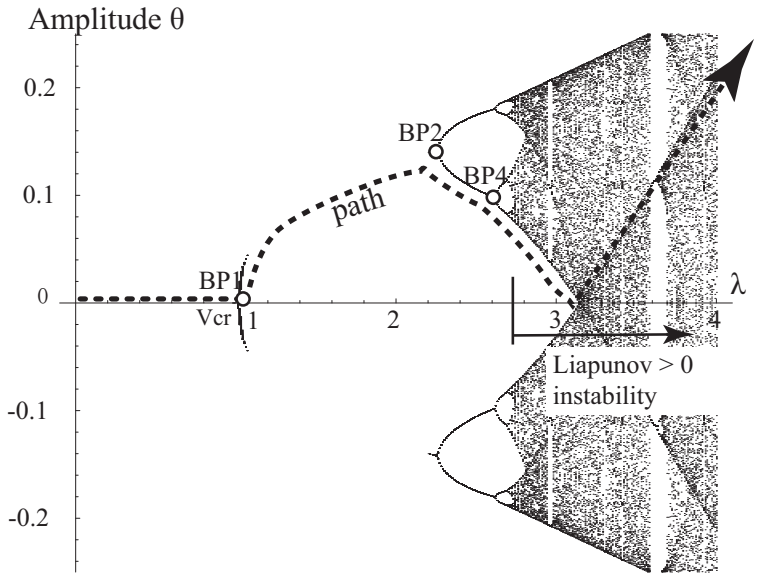

Figure 9: Trend in qualitative changes shown on the bifurcation diagram.

the problem of dynamic instability. If some understanding of the dynamic instability can be gained from the bifurcation diagram, it will be possible to make rough predictions and to understand instability trends without engaging in wind tunnel experiments or large-scale computational fluid dynamics.

5.2. Probability of occurrence of stable discrete solutions

In the chaotic regime, unstable aperiodic solutions occur, and once-appeared solutions take trajectories that do not appear to be in two degrees of freedom. A slight difference in the initial value also greatly affects the trajectory of the solution. However, considering the probability of occurrence of the non-periodic solution, the nature of the generated solution can be considered without being affected by the initial value or the number of calculations. When the system vibrates irregularly, it is important not to track this behaviour but to find how easily it can incline as a whole. Here, we consider the aspect of the solution generated in the chaotic region. From the bifurcation diagram of **Fig.9**, we can also observe the frequency of the solution generated from the shading of its distribution. **Fig.**10 shows the probability of occurrence of stable discrete solutions for each parameter. Figures (a), (b), and (d) represent the probability of occurrence of the aperiodic solution, and Figure (c) shows the probability of occurrence of the solution at the three-period window. From figures (a), (b), and (d), it can be observed that many stable discrete solutions in the chaotic region occur around the maximum and minimum values of displacement and around the centre. **Fig.**11 shows the extracted stable and/or unstable discrete solutions for which the probability of occurrence at the load parameter λ is maximized. Displacement θ of the maximum probability of occurrence after the period-doubling bifurcation indicates that the

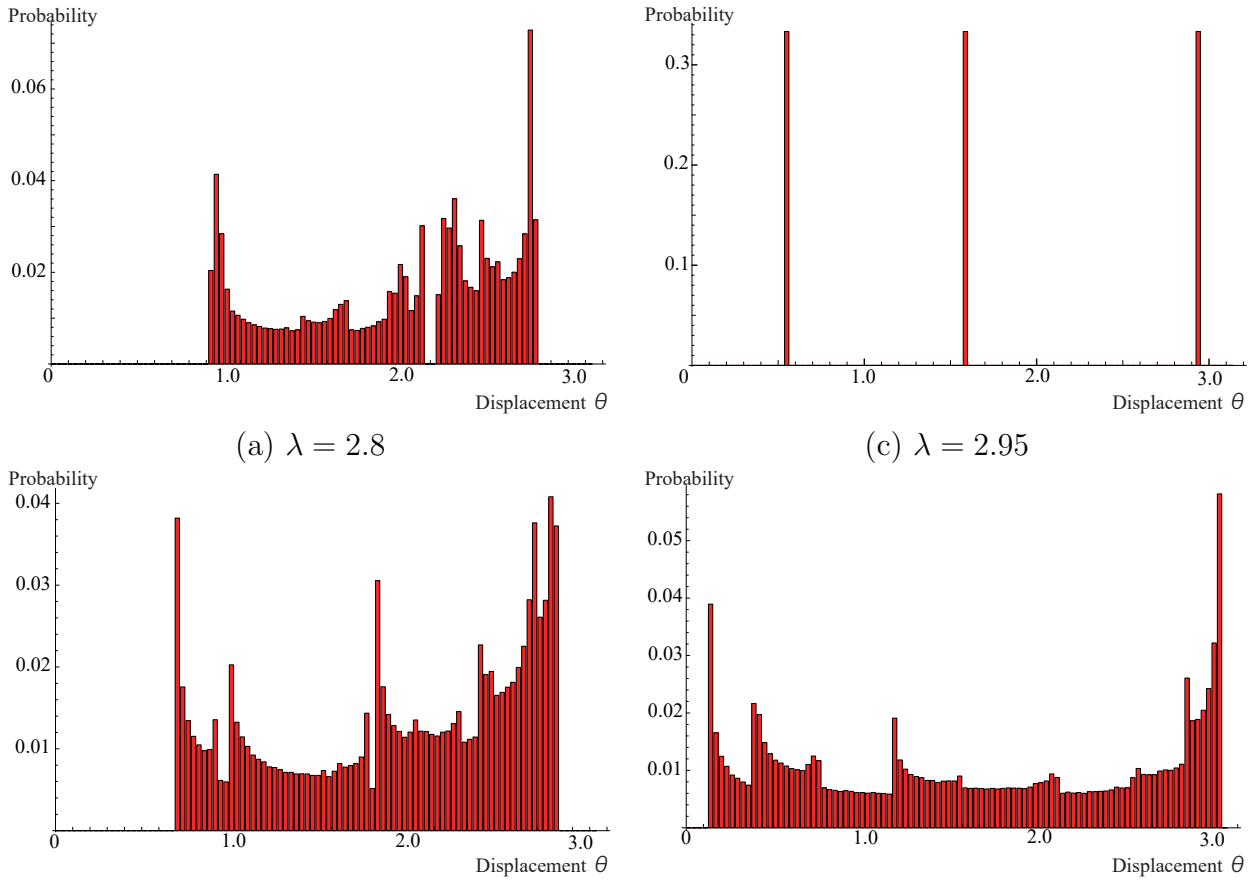

(a) $\lambda = 2.8$

(c) $\lambda = 2.95$

(b) $\lambda = 2.9$

(d) $\lambda = 3.1$

Figure 10: Probability of solution for each λ

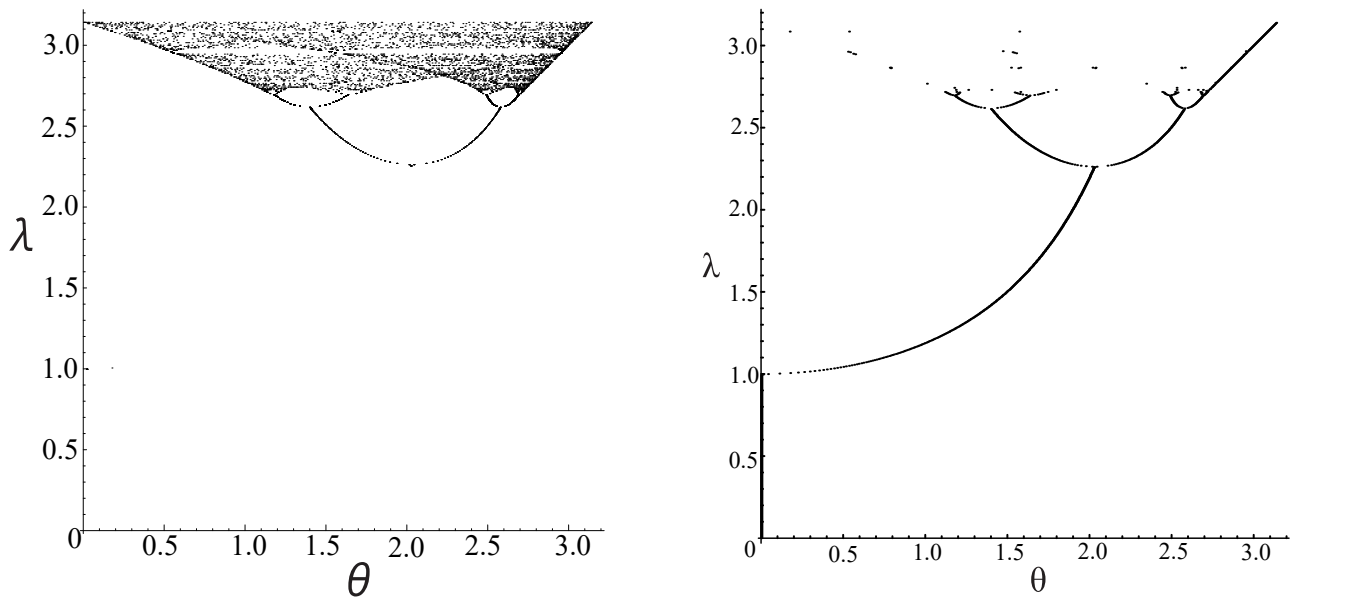

(a) Overall view (b) Path map with maximum occurrence probability

Figure 11: 1-DOF rigid body-spring bifurcation diagram

displacement is maximized within the range in which the solution occurs. From this fact, it can be estimated that the amplitude increases, thus inclining the rod much outward, but the solution is also distributed inward, and it can be said that it contains factors which cause complicated behaviour even in such a simple structural system by some disturbance from the outside.

6. Conclusion

The results from this investigation are summarised as follows.

1. In the flutter experiment in the open channel flow, we observe a critical point in the vibrational response, bifurcation, and turbulent responses as the flow velocity is increased. Thus, we find that a bifurcation problem exists in the interacting fluid-structure system, although it is a non-conservative system. In particular, we observe a strong nonlinearity between the amplitude and the flow velocity above the critical flow velocity.
2. The existing formulation based on the analytical theory of elastohydrodynamics, which describes behaviour near the critical flow velocity, can lead to solution curves, as seen in the averaging method. However, understanding or formulating the subsequent higher-order bifurcation and the solution's behaviour is difficult and depends on the stability and complexity of the solution. Instead, we have attempted to formulate the problem using discrete mechanics. The problem of instability in a non-conservative field has been said to be of no usuful in the static situation; however, we

have developed an analytical approach by introducing discrete mechanics and verified its similarity to the experimental results.

3. The large-scale finite element analysis of vortex excitation under high fluid velocity is difficult. In the present approximate approach, we combine elastohydrodynamics with discrete mechanics to construct a model capable of reproducing the behaviour of structural systems above the critical flow velocity where flutter can occur.
4. We have demonstrated that the complex behaviour of an interacting fluid-structure system can be understood from the broad perspective of discrete mechanics applied to a non-equilibrium system.
5. In this study, we focused on predicting complex behaviour with elastohydrodynamic simulation. However, it is important to investigate flow fields in three-dimensional space as well as in the turbulent regime. It will be interesting to investigate the presence of wakes and of variations in the Strouhal number.
6. Since the main attractor (path) $\theta(\lambda)$ of the maximum probability of occurrence after the period-doubling bifurcation is that the displacement is maximized or minimized within the range in which the solution is occurring. From this fact, it can be estimated that the amplitude increases and vibrates while inclined outward and/or inward, and it can be said that it contains factors which cause complicated behaviour with higher frequency.

Appendix A. Averaging method to get numerical solution

In general, it is not strictly possible to solve kinematic equation with non-linear system except a suitable case to compare with the linear problem is different. Averaging method is a practical method to solve non-linear problem as approximate analysis. It a useful method using a computer and perturbation method.

For example, let us consider a free linear vibration equation without any damping in the following;

$$m\ddot{\theta} + \beta\theta = 0.$$

In this case, using a parameter $\omega^2 = k/m$, we can obtain

$$\theta = a\sin(\omega t + \phi).$$

in where, a and ϕ are integral constants depend on the boundary condition.

If the equation had an imperfection parameter ϵ with a small non-linear function $f(\theta, \dot{\theta})$, it would be expressed as

$$\ddot{\theta} + \omega^2\theta + \epsilon f(\theta, \dot{\theta}) = 0. \tag{A.1}$$

The solution is assumed as

$$\theta = a(t)\sin(\omega t + \phi(t)) \tag{A.2}$$

It is decided $a(t)$ and $\phi(t)$.

STEP 1

Differentiating Eq.(A.2), it is shown as

$$\dot{\theta} = \dot{a}\sin(\omega t + \phi) + a\dot{\phi}\sin(\omega t + \phi) + a\omega\cos(\omega + \phi). \tag{A.3}$$

With small nonlinearity, as it is assumed

$$\dot{a}\sin(\omega t + \phi) + a\dot{\phi}\sin(\omega t + \phi) = 0, \tag{A.4}$$

It becomes

$$\dot{\theta} = a\omega\cos(\omega t + \phi). \tag{A.5}$$

Using two functions $a(t), \phi(t)$, it shows a single degree-of-freedom in Eq.(A.2). We try to obtain $a(t), \phi(t)$ from Eq.(A.2) and Eq.(A.5) in the following;

$$a(t)^2 = \frac{\dot{\theta}^2 + \omega^2\theta^2}{\omega^2}, \tag{A.6}$$

$$\phi(t) = \arctan\left(\frac{\omega\theta}{\dot{\theta}}\right) - \omega t. \tag{A.7}$$

STEP 2

If second order different of θ is carried out, it is expressed in the following;

$$\ddot{\theta} = \dot{a}\omega\cos(\omega t + \phi) - a\omega\dot{\phi}\sin(\omega t + \phi) - a\omega^2\sin(\omega t + \phi) \tag{A.8}$$

Substituting this for Eq.(A.1), we obtain

$$\dot{a}\omega\cos(\omega t + \phi) - a\omega\dot{\phi}\sin(\omega t + \phi) + \epsilon f(\theta, \dot{\theta}) = 0 \tag{A.9}$$

STEP 3

Using Eq.(A.4) and Eq.(A.8), $a(t), \phi(t)$ are shown in the following;

$$\dot{a} = -\frac{\epsilon}{\omega} f(a\sin(\omega t + \phi), a\omega\cos(\omega t + \phi))\cos(\omega t + \phi) \tag{A.10}$$

$$\dot{\phi} = \frac{\epsilon}{a\omega} f(a\sin(\omega t + \phi), a\omega\cos(\omega t + \phi))\sin(\omega t + \phi) \tag{A.11}$$

STEP 4

It would be not possible to solve because Eq.(A.10) and Eq.(A.11) are so complex, we should consider approximate method. As we assumed that ϵ was a small parameter, $\dot{a}$ and $\dot{\phi}$ are small too, and a, ϕ become almost constant for time. Variables a, ϕ on time period $[t, t + 2\pi\omega]$ are replaced to average A, Φ and small change $\delta_a(t), \delta_\phi(t)$ in the following;

$$a(t) = A + \delta_a(t) \tag{A.12}$$

and

$$\phi(t) = \Phi + \delta_\phi(t). \tag{A.13}$$

STEP 5

Neglecting the high-order terms, we carried out the differentiation for them,

$$\dot{a} = -\frac{\epsilon}{\omega} f(A\sin\gamma, A\omega\cos\gamma)\cos\gamma, \tag{A.14}$$

and

$$\dot{\phi} = \frac{\epsilon}{A\omega} f(A\sin\gamma, A\omega\cos\gamma)\sin\gamma, \tag{A.15}$$

$$\gamma = \omega t + \Phi \tag{A.16}$$

in where, we use a variable γ to prepare the integration.

STEP 6

After we solve the following equations;

$$\dot{A} = -\frac{\epsilon}{2\pi\omega}\int_0^{2\pi} f(A\sin\gamma, A\omega\cos\gamma)\cos\gamma d\gamma \tag{A.17}$$

$$\dot{\Phi} = \frac{\epsilon}{2\pi A\omega}\int_0^{2\pi} f(A\sin\gamma, A\omega\cos\gamma)\sin\gamma d\gamma \tag{A.18}$$

They are decided A, Φ, hence they are transported to $a(t), \phi(t)$ to solve the initiated nonlinear kinematic equation, finally.

Acknowledgement: Prof. Takanori SAGA and Prof. Katsutoshi WATANABE in Tokuyama College of Technology and my student Ronny were greatly supported by experimental works.

References

[1] Chen S.R. and Cai C.S. , Evolution of long-span bridge response to wind-numerical simulation and discussion, Computers and Structures 81 (2003) p.2055-2066.

[2] Øiseth O., Rönnquist A. and Sigbjörnsson R. , Simplified prediction of wind-induced response and stability limit ofslenderlong-span suspension bridges, basedon modified quasi-steadytheory : A case study, Journal of Wind Engineering and Industrial Aerodynamics, 98 (2010) p.730-741.

[3] Huseyin, K. , Nonlinear Theory of Elastic Stability, Noordhoff, Leyden, 1974.

[4] Thompson, J.M.T. and Hunt, G.W. , Static and Dynamic Instabilities in the physical sciences, an inaugural lecture, *J. Eng. Sci., Univ. Riyadh*, 6(71) 1980.
J.M.T. Thompson, Static and dynamic instabilities in the physical sciences, J. Eng. Sci., Univ. Riyadh, 6, 71-96 (1980).

[5] Andronov, A.A., Leontovich, E.A., Gordon, I.I., and Maier, A.G., Theory of Bifurcations of Dynamical Systems on a Plane and Qualitative Theory of order Dynamical Systems, *Wiley, New York*, 1971.

[6] Bolotin, V.V. , Nonconservative Problems of the Theory of Elastic Stability, Pergamon Press, Oxford, 1963.

[7] Rosenberg, R.M. , On nonlinear vibration of systems with many degrees of freedom, *Adv. Appl. Mech.*, 9 (1966) 156-243.

[8] Huchinson, J.W. and Budiansky, B. , Dynamic buckling estimates, *AIAA J.*, 4 (1966) 525-530.

[9] Nayfeh, A.H. and Mook. D.T. , Nonlinear Oscillations, *John Wiley & Sons*, 1979.

[10] Nayfeh, A.H. and Sanchez , Bifurcations in a Forced Softening Duffing Oscillator, International Journal of Nonlinear Mechanics, 24(6) (1989) p.483-497.

[11] Plaut, R.H. , Postbuckling analysis of nonconservative elastic systems, *J. Struct. Mech.*, 4 (1976) 395-416.

[12] Plaut, R.H. , Branching analysis at coincident buckling loads of nonconservative elastic systems, *J. Appl. Mech.*, 44 (1977) 317-321.

[13] Huseyin, K. and Mandadi, V. , On the instability of multiple-parameter systems, Sectional Lecture, *Proc. Fefteenth Internatinal Cong. Theoretical and Appl. Mech., Toronto*, 1980.

[14] Thompson, J.M.T. and Hunt, G.W. , A General Theory of Elastic Stability, Wiley, London, 1973.

[15] Novak, M. , Galloping and vortex induced oscillations of structures, *Proc. third International Conf. on Wind Effects on Buildings and Structures*, Science Council of Japan, Tokyo, 1971.

[16] Parkinson, G.V. and Brooks, N.P.H. , On the aeroelastic instability of bluff cylinders, *J. Appl. Mech.*, 28 (1961) 252-258.

[17] Parkinson, G.V. and Smith, J.D. , The square prism as an aeroelastic non-linear oscillator, *Quart. J. Mech. and Appl. Math.*, 17(225), 1964.

[18] Matsuda, H., Sakiyama T. and Morita, C. : Variable Cross Sectional Beck's Column Subjected to Nonconservative Load, *ZAMM, Z, angew. Math. Mech.*, 73 (1993) p.383-385.

[19] Honma, T., Tosaka N. , Dynamic stability analysis of the elastic bar which receives non-preservability external force, *Journal of Structural and Construction Engineering (in Japanese)*, 461 (1994) p.37-46.

[20] Miyata, T. , Realization and its windproof stability of an overly huge new style type bridge, *Proceedings of Structure and materials in Civil Engineering (in Japanese)*, 13 (1997) p.1-12.

[21] Matsumoto, M., Ohhigashi, Y., Shiratsuchi H., Aoki, J., Fujii, T. , Research on the turbulent flow effect exerted on whirlpool excitation of a bridge standard section, *Journal of Structural Engineering in Civil Engineering in Japanese Society of Civil Engineers (in Japanese)*, 42A (1996) p.813-818.

[22] Kazama, K., Miyata, T. and Yamada, K. , Research on the flutter characteristic accompanying longer of a suspension bridge, *Journal of Structural Engineering in Civil Engineering in Japanese Society of Civil Engineers (in Japanese)*, 41A (1995) p.809-816.

[23] Yoneda, M., Ohno, K., Tamaki, Y. and Kimura, M. , The effect of perpendicular crossing stayed exerted on the coupling flutter characteristic of overly huge box beam type of suspention bridge, – The optimal position in case of measurement by air dynamics– , *Journal of Structural Engineering in Civil Engineering in Japanese Society of Civil Engineers (in Japanese)*, 44A (1998) p.907-916.

[24] Kawamoto, H. and Yoshida H. , Coupling analysis between fluid-structure for a three-dimensional elastic pillar, *Journal of Structural Mechanics and Earthquake Engineering(I) (in Japanese)*, No.668, I-54 (2001) p.195-206.

[25] Dowell, E.H., Non-linear oscillations of a fluttering plate, AIAA J., 4 (1966) p.1267-1275.

[26] Dowell, E.H., Aero-elasticity of lates and Shells, Noordhoff, Leyden, 1975.

[27] Moon, F.C. and Holmes, P.J. , A magnetoelastic strange attractor, *Journal of Sound and Vibration*, 65(2) (1979) p.275-296.

[28] Ueda, Y. , Steady motions exhibited by Duffing's equation , A picture book of regular and chaotic motions, *In New Approaches to Nonlinear Problems in Dynamics, SIAM* (1980) p.311-322.

[29] Ario, I., Homoclinic bifurcation and chaos attractor in elastic two-bar truss. *Int. J. Non-Linear Mechanics*, 39(4) (2004) p.605-617.

[30] Ario, I. , Hierarchical Structural Analysis for the Multi-folding Structures with Hill-top Bifurcation Points, *Proceedings of IUTAM Symposium on 50 Years of Chaos , International Union of Theoretical and Applied Mechanics*, Kyoto (2011).

[31] Arnold, V.I. , Geometrical methods in the theory of ordinary differential equations, *Springer-Verlag, New York*, 1983.

[32] Thompson, J.M.T. and Stewart, H.B. , Nonlinear dynamics and chaos geometical methods for engineers and scientists, *John Wiley & Sons Ltd.*, 1986.

[33] Wiggins, S. , Introduction to applied nonlinear dynamical systems and chaos, *Springer-Verlag, New York*, 1990.

[34] La Salle, J. and Lefschetz, S. , STABILITY BY LIAPUNOV'S DIRECT METHOD With Applications, *Academic Press, Inc.*, 1961.

[35] Ario, I., Multiple duffing problem in a folding structure with hill-top bifurcation, *Chaos, Solitons & Fractals*, 51 (2013) p.52-63.

[36] Ario, I., Multiple Duffing problem in a folding structure with hilltop bifurcation and possible imperfections, *Meccanica*, **49**,8 (2014) p.1967-1983.